The terdiurnal tide in the MUAM circulation model

A. Krug, F. Lilienthal, Ch. Jacobi

Institute for Meteorology, Stephanstr. 3, 04103 Leipzig
E-Mail: amelie.krug@studserv.uni-leipzig.de

Summary: The terdiurnal tide (TDT) in the mesosphere and lower thermosphere has been simulated with a 3D mechanistic circulation model of the middle atmosphere. The tidal temperature amplitude shows a clear seasonal cycle with peaks in the midlatitudes and near the equator at equinox. Under solstice conditions maximum amplitudes occur at 10° in the summer hemisphere and at 30-40° latitude in the winter hemisphere. The vertical wavelengths are large at midlatitudes and small at the equator with about 15 km. These characteristics are compared with SABER/TIMED satellite data from 2002-2009. Especially for temperature amplitudes good agreement is visible. At 90 km, comparison of the zonal wind TDT with radar observations from the literature also shows that the model realistically simulates the seasonal cycle of the TDT.

Zusammenfassung: Die achtstündige Gezeit (TDT) in der Mesosphäre und unteren Thermosphäre wurde mit einem 3D mechanistischen Zirkulationsmodell der mittleren Atmosphäre modelliert. Die Amplitude der achtstündigen Gezeit in der Temperatur zeigt dabei eine klare saisonale Variabilität mit Maxima im Bereich der mittleren Breiten und des Äquators während der Äquinoktien. Die vertikale Wellenlänge ist in den mittleren Breiten groß und am Äquator mit ca. 15 km klein. Diese Strukturen werden mit SABER/TIMED Satellitenmessungen der Jahre 2002-2009 verglichen. Vor allem für die Amplituden in der Temperatur ist eine gute Übereinstimmung zu erkennen. Ein Vergleich der achtstündigen Gezeit im Zonalwind in 90 km Höhe mit Radarmessungen aus der Literatur zeigt, dass das Modell den Jahresgang realistisch simuliert.

1 Introduction

Mesosphere and lower thermosphere (MLT) large-scale dynamics are considerably influenced by atmospheric waves, including solar tides, which are inertial gravity waves with periods of a solar day or its subharmonics. Solar tides are forced by absorption of solar radiation mainly by ozone in the stratosphere and water vapor in the troposphere. Atmospheric tides propagate in each spatial direction with vertical growing amplitudes owing to the exponentially decreasing density with height. Therefore, tidal components attain large amplitudes in the MLT (Chapman and Lindzen, 1970; Andrews et al., 1987). In this article, the westward propagating TDT with a zonal wavenumber of s=3 (TW3) is presented. The TW3 generally has smaller amplitudes than the semidiurnal (SDT) and diurnal tide (DT). Beside solar heating, other formation mechanisms of terdiurnal tides have been proposed, such as gravity wave breaking (Miyahara and Forbes, 1991) and nonlinear interactions between DT and SDT (Teitelbaum et al., 1989). There have

been several studies of terdiurnal signatures in radar and satellite measurements. Beldon et al. (2006) were investigating horizontal winds, measured by a VHF meteor radar at Castle Eaton, UK (52.6° N, 2.2° W), near 90 km in 1988-2004, found a clear seasonal behavior with largest amplitudes in autumn and early winter. A similar seasonal cycle was observed by Fytterer and Jacobi (2011) and Jacobi and Fytterer (2012) over Collm (51.3° N; 13.0° E). In meteor radar measurements over Wakkanai (45.4° N; 141.7° E), however, slightly larger amplitudes were observed in winter than in summer (Namboothiri et al., 2004).

Yue et al. (2013) analyzed measurements by the Sounding of the Atmosphere using Broadband Emission Radiometry (SABER) and the TIMED Doppler Interferometer (TIDI) instruments onboard the Thermosphere-Ionosphere-Mesosphere-Energetics and Dynamics (TIMED) satellite from 2002-2009. TIDI horizontal wind measurements reveal amplitudes of more than 16 ms^{-1} at 50° N/S above 100 km and an additional peak of the meridional component in ~82 km and 10-20° N is visible. SABER temperature terdiurnal amplitudes match to the first real symmetric (3,3) mode with peaks up to 8 K above the equator and at midlatitudes. SABER/TIMED data of 2002-2011 were also analyzed by Moudden and Forbes (2013). Here, for an altitude of about 90 km, largest amplitudes were found above the equator during equinox and at 60° N during May (~7 K) and 60° S in October (up to 5 K). Generally, TDT amplitudes at midlatitudes tend to maximize during equinox and in winter. Near the equator, there is an annual cycle with largest amplitudes in summer.

Modeling of the TDT so far has mainly been focused on excitation mechanisms, in particular direct solar heating and nonlinear interaction between DT and SDT. Huang et al. (2007) developed a nonlinear numerical tidal model to investigate amplitude features of the TDT excited by nonlinear interaction between DT and SDT. The results suggest that the migrating TDT can be significantly excited by this mechanism in the MLT region. Du and Ward (2010) analyzed CMAM Global Circulation Model results with regard to correlations between TDT and DT/SDT on the short-term or seasonal time scale. Correlation analysis indicated that nonlinear forcing is unlikely to be the source of the migrating TDT in the CMAM. Akmaev (2001) concluded from circulation model calculations that nonlinear interaction makes a contribution to the excitation of the TDT at 95-100 km, particularly during equinox. Smith and Ortland (2001) performed similar calculations as well as numerical runs in which the SDT forcing was removed from the model in order to exclude nonlinear forcing as possible TDT source. The results indicate that the direct solar heating is the main driver of the TDT at middle and high latitudes, while nonlinear interactions contribute to the TDT at low latitudes.

In this paper we use the Middle and Upper Atmosphere Model (MUAM; Pogoreltsev et al., 2007) to simulate TDT amplitudes and phases. The remainder of this paper is organized as follows: In the following section 2 the model is described, in section 3 the seasonal cycle of the tidal amplitudes in temperature and zonal wind at an approximate height of 90 km are presented. Furthermore, altitude-latitude cross sections of terdiurnal amplitudes and phases in zonal wind and in temperature are shown under equinox and solstice conditions. Tidal structures in temperature are compared with observations, in particular with SABER/TIMED temperature measurements between 2002-2009, as presented in Pancheva et al. (2013). Section 4 concludes the paper.

2 Model description

MUAM (Pogoreltsev et al., 2007) is a 3D nonlinear mechanistic grid point model which generates atmospheric circulation self-consistently. The horizontal resolution in latitude and longitude is $5° \times 5.625°$. In the vertical, a log-pressure height $z = -H \ln(p/p_0)$ with a constant scale height H of 7 km and a reference pressure $p_0 = 1000$ hPa is used. Throughout the middle atmosphere, log-pressure heights and geometric heights do not differ much. The 56 vertical layers extend to an altitude of about 160 km. For time integration an Euler backward scheme after Matsuno (1966) is included with 16 time steps per hour.

As lower boundary condition we assimilate zonally averaged geopotential and temperature fields, and additionally, monthly averaged amplitudes and phases of the first three harmonics as stationary planetary waves, both taken from ERA-Interim Reanalysis data

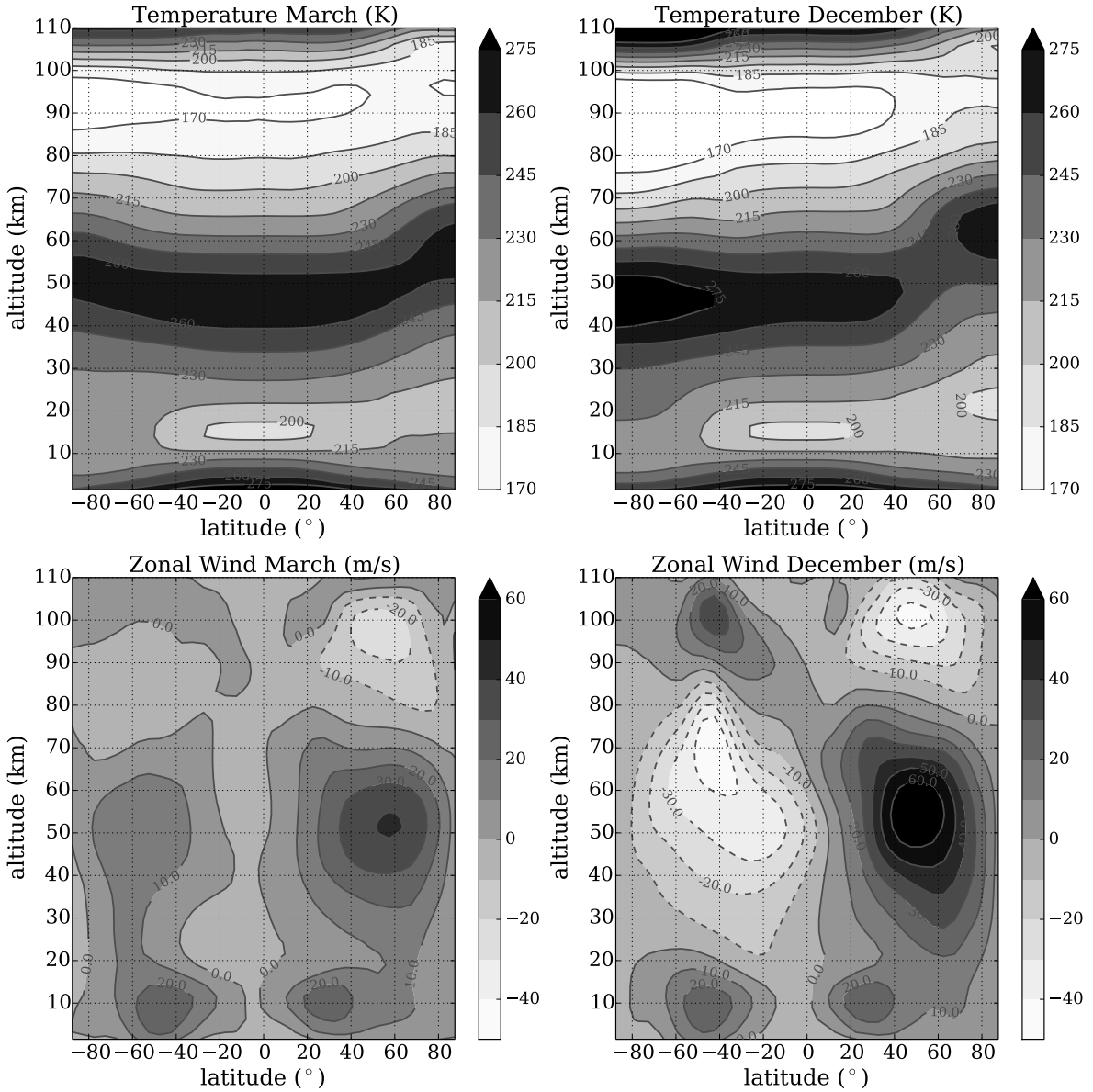

Fig. 1: MUAM zonal mean background temperature (upper row) and zonal wind (lower row) in March and December.

(Dee et al., 2011) at 1000 hPa. We further nudge zonally averaged ERA-Interim Reanalysis temperature data up to 30 km log-pressure height. Here, a 11-year monthly mean of 2000 to 2010 is applied.

Heating of the atmosphere due to absorption of solar radiation by ozone and molecular oxygen are included according to Strobel (1978) and Mlynczak and Solomon (1993). Heating rates of CO_2 are adjusted according to Liou (1992) and water vapor is included after Freidenreich and Ramaswamy (1999). EUV-heating rates are parameterized after Richards et al. (1994) and Roble (1995). Infrared cooling of CO_2 in the 15μm band in the stratosphere and lower mesosphere is calculated after Fomichev et al. (1998), cooling of water vapor after Chou et al. (1993). Ozone infrared cooling, which is mainly dominant at the lower mesosphere near the stratopause in the 9,6 μm band, is applied after Fomichev and Shved (1985). More specific information may be found in Lange (2001), section 2.1.2 and Fröhlich et al. (2003).

In MUAM, water vapor and ozone fields are prescribed. While water vapor is given as a simple zonal mean distribution, we use monthly means of ozone data by Stratosphere-troposphere Processes and their Role in Climate Project (SPARC; Randel and Wu, 2015) up to a height of 50 km log-pressure. That means that no secondary ozone maximum is considered. CO_2 is included by monthly means of measurements by Mauna Loa Observatory (Dlugokencky et al., 2014). For the presented climatology, measurements of ozone and CO_2 in 2005 are used.

The model is initialized with a global uniform temperature profile and zero wind. In a 120 model day spin-up phase, the mean wind fields are built up. In the course of this, solar heating rates are averaged over longitudes, so that no tides are forced. After that phase, during another 210 days the tides are formed by allowing longitudinal dependent solar heating. Thereafter, for each model run, additional 30 model days are simulated for January and July conditions with declination set to the respective month. Here, we analyze the TW3 in temperature and zonal wind from these 30 model days here.

The model results for zonal mean background temperature and zonal wind are shown in Figure 1. Altitude is given in geometric heights. Modeled background fields well represent the mean climatology of the middle atmosphere as, e. g., given by the COSPAR International Reference Atmosphere (CIRA; Chandra et al., 1990). In March zonal wind reverses in an altitude of ~70-80 km and reaches 40 ms^{-1} in 50 km altitude at ~60° N. In December, the wind reversal occurs slightly higher at 80-90 km. Wind speeds range from more than 40 ms^{-1} westward to ~70 ms^{-1} eastward.

3 Model results for the terdiurnal tide

To give an overview of the seasonal and latitudinal behavior, modeled tidal amplitudes in temperature and zonal wind are shown in Figure 2 at 90 km. At low latitudes, amplitudes are large during summer and the equinoxes. This pattern is also seen by Pancheva et al. (2013) but for higher altitudes. At lower midlatitudes amplitudes are increased in winter (~1 K). Weaker peaks are visible in June-July and August-September in the Northern Hemisphere (NH) and April/September in the Southern Hemisphere (SH) (~0.75 K). The SH winter maximum has also been modeled by Yue et al. (2013), while the pattern in the NH has not been modeled by them. The equinox maxima, however, has been observed by Pancheva et al. (2013) using SABER data. On the right panel in Figure 2

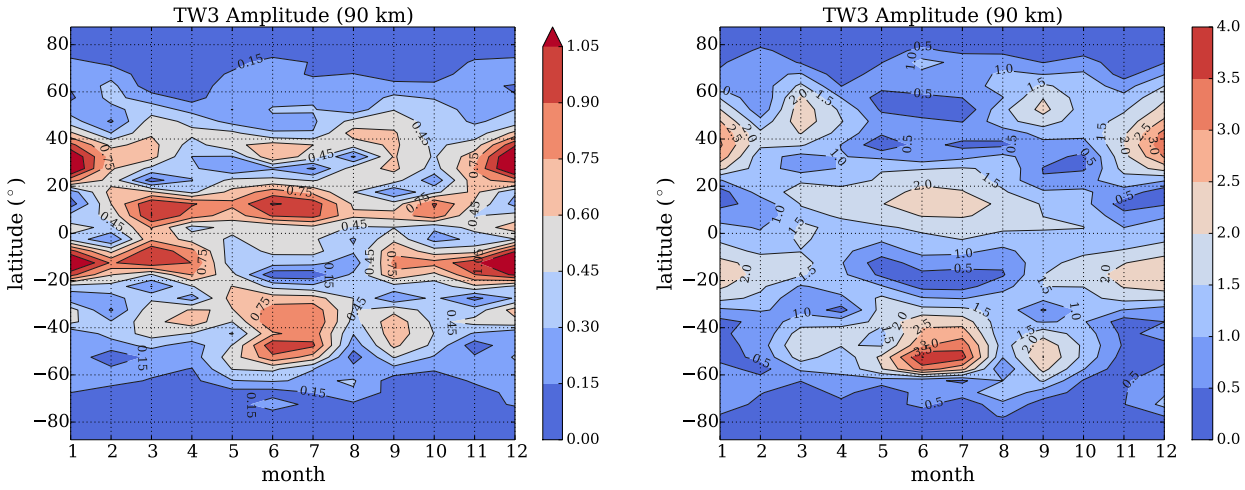

Fig. 2: Latitude-time cross section of the terdiurnal amplitudes in temperature (left, in K) and zonal wind (right, in ms^{-1}*) at 90 km modeled with MUAM.*

terdiurnal zonal wind amplitudes are presented. Similar to temperature amplitudes, peaks in winter and, for the NH, during equinox are visible at midlatitudes and in summer at low latitudes. This is in good agreement with TIDI TW3 amplitudes presented in Yue et al. (2013). The equinox and winter maxima at NH midlatitudes have also been registered by radar (Beldon et al., 2006; Fytterer and Jacobi, 2011). The equinox maxima, which are clearly observed in satellite and ground-based data, are not observed in other models like TIME-GCM (Yue et al., 2013) or the extended Canadian Middle Atmospheric Model (CMAM; Du and Ward, 2010). We may conclude that the seasonal cycle of the TW3 amplitudes in temperature and zonal wind can be well reproduced by MUAM. However, modeled amplitudes are smaller than the observed ones by a factor of two at most.

In the following, we directly compare our modeled TDT amplitudes with SABER analyses by Pancheva et al. (2013). The modeled tidal amplitudes during equinox and solstice are presented in Figure 3 as black solid lines. SABER TW3 amplitudes from Pancheva et al. (2013) are given in the figure as color coding. In order to allow comparability with SABER observations that are only available up to 50° latitude, only the region from 50° S to 50° N is shown here. During equinox (upper row) maxima in the midlatitudes (~3-5 K) and above the equator (~6 K) are visible. In June the tidal amplitude shows peaks at 10° N (~7 K), 30° N (~4 K) and 40° S (~5 K). The amplitude maximizes at 10° S (~9 K) and 30° N/S (~5 K) in December.

By comparing MUAM results with SABER measurements, the good general correspondence between the latitudinal distribution of observed and modeled amplitudes is striking. The observed amplitudes are slightly higher (~2 K), but the latitudinal and seasonal structures are well reproduced by MUAM. Even the weak peak around 85-90 km above the equator is evident in MUAM, though the modeled amplitudes are about 3 K too small. Pancheva et al. (2013) claim that this peak corresponds to a trapped phase above the equator. This can be seen in Figure 4, which presents a altitude-latitude cross section of the tidal phase structure in SABER/TIMED measurements (color shaded) and MUAM (black solid lines).

Observed tidal phase shows large vertical wavelengths above the equator and small ones in midlatitudes (e. g. from 70 km to 95 km at 40° S in March). Overall, a negative phase gradient can be seen, which implies upward propagating energy. This is similar to MUAM results. However, the modeled phases have shortest vertical wavelengths above the equator with ca. 15 km in March and from 90 to 100 km above the equator in October or at 10° S in June. In contrast, vertical wavelengths at midlatitudes are large. The modeled phases in the NH and SH in summer and winter are similar, as is the case with the amplitudes during solstice.

The modeled TW3 zonal wind amplitudes in March and December are displayed in Figure 5. In March maximum values with up to 9 ms^{-1} are reached in the midlatitudes and above the equator. In the SH peaks are slightly shifted to low and high latitudes in December. Like TW3 temperature phases, shown in Figure 4, TW3 zonal wind phases have large wavelengths above the equator and smaller ones in the midlatitudes.

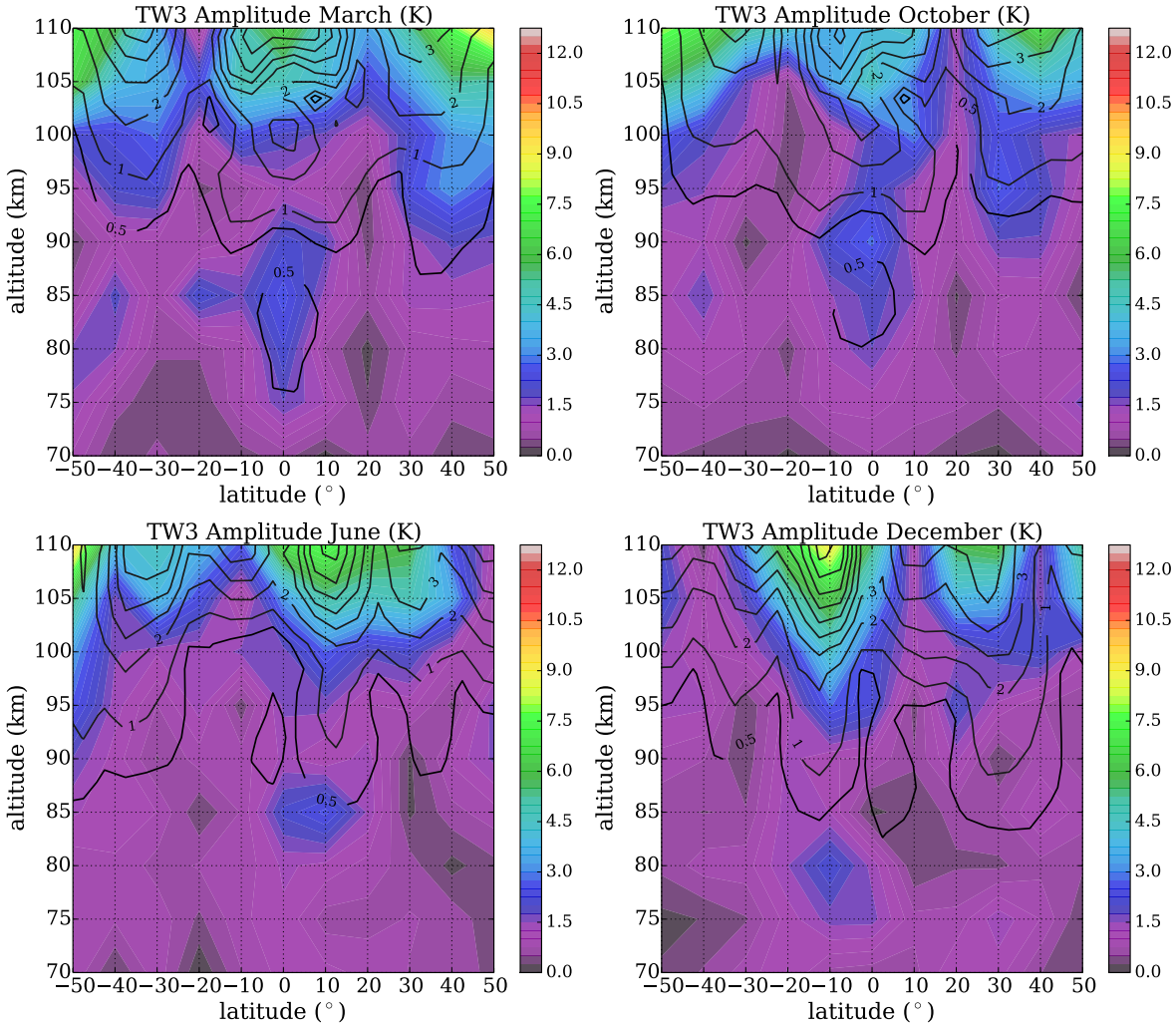

Fig. 3: Terdiurnal temperature amplitudes for equinox (upper row) and solstice (lower row) conditions modeled with MUAM. Corresponding SABER amplitudes from Pancheva et al. (2013) are added in color.

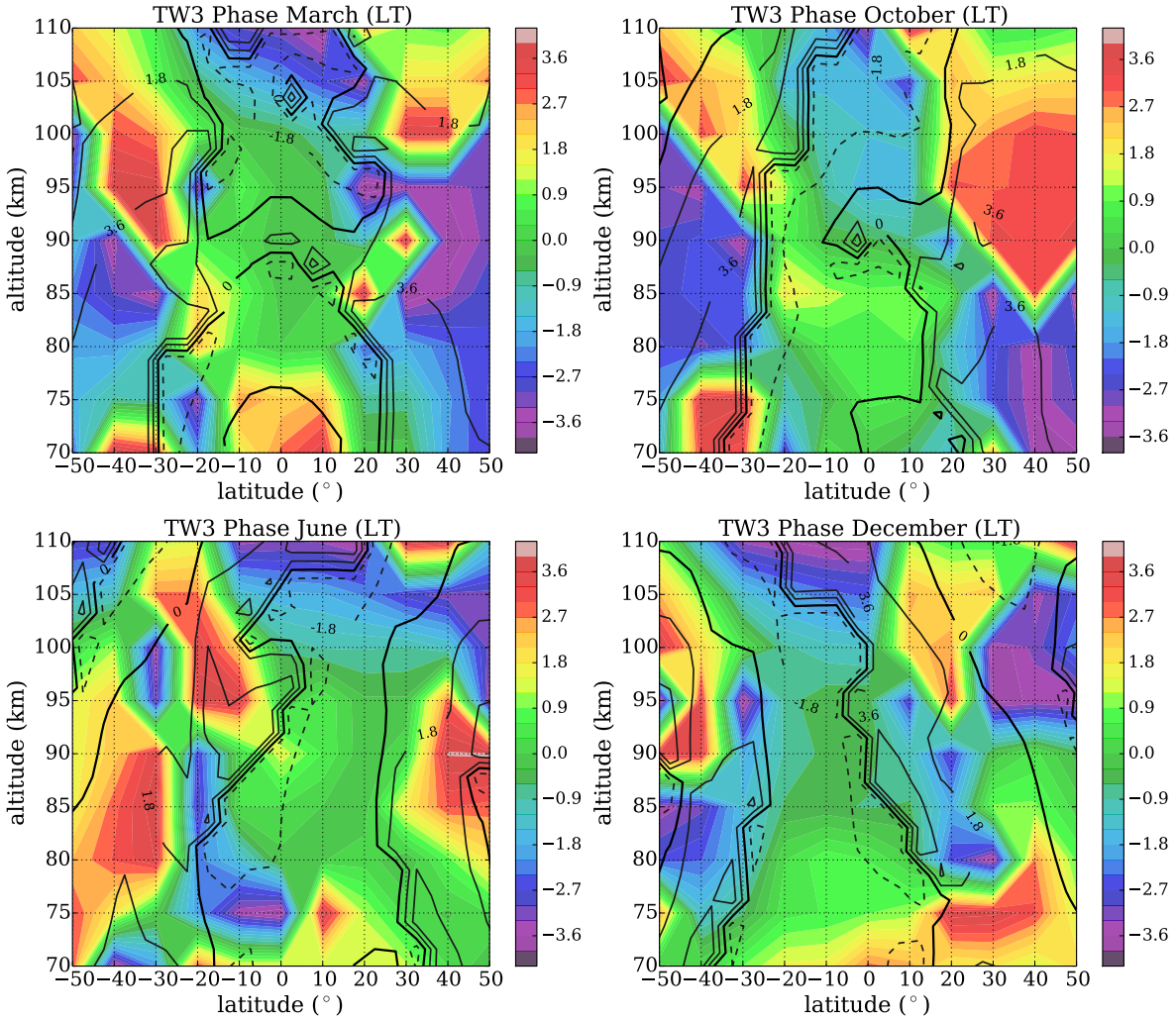

Fig. 4: As in Figure 3, but for the terdiurnal temperature phases.

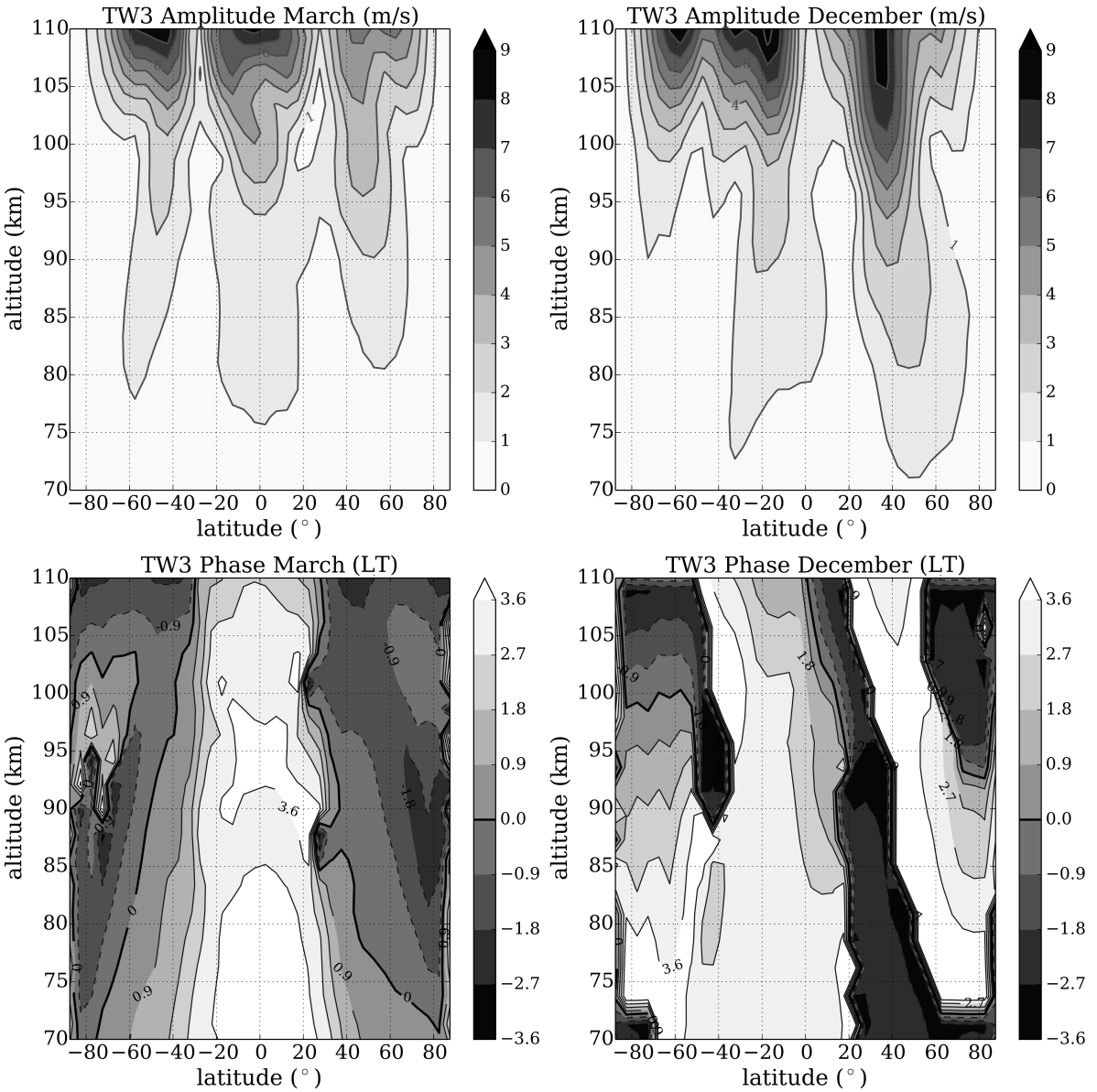

Fig. 5: Terdiurnal zonal wind amplitudes (upper row) and phases (lower row) for March and December modeled with MUAM.

4 Conclusions

We have analyzed the TW3 amplitudes and phases as simulated by the Middle and Upper Atmosphere Model. For modeling the TW3 realistically, lower atmosphere circulation has been included by assimilating 11-year mean ERA-Interim Reanalysis data from 2000-2010. For appropriate heating rates ozone and CO_2 fields according to measurements in 2005 were included.

The seasonal cycle of TW3 temperature and zonal wind amplitudes are shown at an altitude of ~90 km. Good agreement with SABER and TIDI measurements (Yue et al., 2013; Pancheva et al., 2013) is visible. In particular, the midlatitude peak during equinox, which is well expressed in satellite but also in radar observations, is reproduced by MUAM.

Additional to latitude-time cross sections, the tidal structures in temperature are presented for equinox and solstice conditions between 50° N/S in an altitude from 70 km to 110 km. Largest amplitudes are found in December at 10° S and ~110 km with more than 9 K. Another peak occurs at 30° N in December. Amplitudes in June are similar to those in December mirror inverted to the equator. Under solstice conditions tidal amplitude maximizes above the equator and at midlatitudes with up to 6 K. Modeled TW3 phases have shortest vertical wavelengths above the equator from ~87 km to 100 km in March and from 90 to 100 km in October or at 10° S in June. In contrast, vertical wavelengths at midlatitudes are large.

These results were compared with SABER/TIMED satellite data (2002-2009). Observed tidal phases show larger vertical wavelengths above the equator. One reason might be that equatorial waves like the quasi-biennial oscillation or Kelvin-waves are not excited in the presented model run. Good agreement in latitudinal structure and maximum values of TW3 amplitudes was found. Even the weak peak at ~85 K above the equator could be reproduced, however, the modeled amplitudes are too weak here.

Generally, the modeled amplitudes are smaller than observed. This might be due to a too strong dissipative damping in the modeled mesosphere and thermosphere. Further experiments will take that into account.

Acknowledgements

The authors are grateful to D. Pancheva for providing SABER/TIMED terdiurnal amplitudes and phases in SABER/TIMED measurements. The work has partly been supported by DFG under grant JA 836/30-1.

References

Akmaev, R. A., 2001: Seasonal variations of the terdiurnal tide in the mesosphere and lower thermosphere: a model study, Geophysical Research Letters, 28, 3817–3820, doi: 10.1029/2001GL013002.

Andrews, D. G., Holton, J. R., and Leovy, C. B., 1987: Middle Atmosphere Dynamics, Academic Press Inc. (London) Ltd., 150-169.

Beldon, C. L., Muller, H. G., and Mitchell, N. J., 2006: The 8-hour tide in the mesosphere and lower thermosphere over the UK, 1988-2004, Journal of Atmospheric and Solar-Terrestrial Physics, 68, 655–668, doi: 10.1016/j.jastp.2005.10.004.

Chandra, S., Fleming, E. L., Shoeberl, M. R., and Barnett, J. J., 1990: Monthly mean global climatology of temperature, wind, geopotential height and pressure for 0–120 km, Advances in Space Research, 10, 3–12, doi: 10.1016/0273-1177(90)90230-W.

Chapman, S. and Lindzen, R., 1970: Atmospheric tides - thermal and gravitational, D. Reidel Publishing Company (Dordrecht, Holland), iX, p. 200.

Chou, M.-D., Ridgway, W. L., and Yan, M. M.-H., 1993: One-Parameter Scaling and Exponential-Sum Fitting for Water Vapor and CO_2 Infrared Transmission

Functions, Journal of the Atmospheric Sciences, 50, 2294–2303, doi:10.1175/1520-0469(1993)050<2294:OPSAES>2.0.CO;2.

Dee, D. P., Uppala, S. M., Simmons, A. J., Berrisford, P., Poli, P., Kobayashi, S., Andrae, U., Balmaseda, M. A., Balsamo, G., Bauer, P., Bechtold, P., Beljaars, A. C. M., van de Berg, L., Bidlot, J., Bormann, N., Delsol, C., Dragani, R., Fuentes, M., Geer, A. J., Haimberger, L., Healy, S. B., Hersbach, H., Hólm, E. V., Isaksen, L., Kållberg, P., Köhler, M., Matricardi, M., McNally, A. P., Monge-Sanz, B. M., Morcrette, J.-J., Park, B.-K., Peubey, C., de Rosnay, P., Tavolato, C., Thépaut, J.-N., and Vitart, F., 2011: The ERA-Interim reanalysis: configuration and performance of the data assimilation system, Quarterly Journal of the Royal Meteorological Society, 137, 553–597, doi: 10.1002/qj.828, Path: http://apps.ecmwf.int/datasets/data/interim_full_moda/?levtype=pl.

Dlugokencky, E., Lang, P., Masarie, K., Crotwell, A., and Crotwell, M., 2014: Atmospheric Carbon Dioxide Dry Air Mole Fractions from the NOAA ESRL Carbon Cycle Cooperative Global Air Sampling Network, 1968-2013, Version: 2014-06-2, Path: ftp://aftp.cmdl.noaa.gov/data/trace_gases/co2/flask/surface/.

Du, J. and Ward, W. E., 2010: Terdiurnal tide in the extended Canadian Middle Atmospheric Model (CMAM), Journal of Geophysical Research, 115, doi:10.1029/2010JD014479, doi: 10.1029/2010JD014479.

Fomichev, V. and Shved, G., 1985: Parameterization of the radiative flux divergence in the 9.6 μm O_3 band, Journal of Atmospheric and Terrestrial Physics, 47, 1037 – 1049, doi: 10.1016/0021-9169(85)90021-2.

Fomichev, V. I., Blanchet, J.-P., and Turner, D. S., 1998: Matrix parameterization of the 15 μm CO_2 band cooling in the middle and upper atmosphere for variable CO_2 concentration, Journal of Geophysical Research: Atmospheres, 103, 11 505–11 528, doi: 10.1029/98JD00799.

Freidenreich, S. M. and Ramaswamy, V., 1999: A new multiple-band solar radiative parameterization for general circulation models, Journal of Geophysical Research: Atmospheres, 104, 31,389–31,409, doi:10.1029/1999JD900456.

Fröhlich, K., Pogoreltsev, A., and Jacobi, Ch.., 2003: The 48 Layer COMMA-LIM Model: Model description, new aspects, and Climatology, Rep. Inst. Meteorol. Univ. Leipzig, 30, 157–185.

Fytterer, T. and Jacobi, Ch.., 2011: Climatology of the 8-h tide over Collm (51.3°N;13°E), Wiss. Mitteil. Inst. f. Meteorol. Univ. Leipzig, 48, 23–32.

Huang, C., Zhang, S., and Yi, F., 2007: A numerical study on amplitude characteristics of the terdiurnal tide excited by nonlinear interaction between the diurnal and semidiurnal tides, Earth, Planets and Space, 59, 183–191.

Jacobi, C. and Fytterer, T., 2012: The 8-h tide in the mesosphere and lower thermosphere over Collm (51.3°N;13°E), 2004-2011, Advances in Radio Science, 10, 265–270, doi:10.5194/ars-10-265-2012, doi: 10.5194/ars-10-265-2012.

Lange, M., 2001: Modellstudien zum CO_2-Anstieg und 0_3-Abbau in der mittleren Atmosphäre und Einfluss des Polarwirbels auf die zonale Symmetrie des Windfeldes in der Mesopausenregion, (Dissertation) University of Leipzig, p. 124.

Liou, K.-N., 1992: Radiation and Cloud Processes in the Atmosphere: Theory, Observation and Modeling, Oxford Monographs on Geology and Geophysics.

Matsuno, T., 1966: Numerical Integrations of the Primitive Equations by a Simulated Backward Difference Method, Journal of the Meteorological Society of Japan, 44, 76–84.

Miyahara, S. and Forbes, J. M., 1991: Interactions between gravity waves and the diurnal tide in the mesosphere and lower thermosphere, Journal of the Meteorological Society of Japan, 69, 523–531.

Mlynczak, M. G. and Solomon, S., 1993: A detailed evaluation of the heating efficiency in the middle atmosphere, Journal of Geophysical Research: Atmospheres, 98, 10 517–10 541, doi: 10.1029/93JD00315.

Moudden, Y. and Forbes, J. M., 2013: A decade-long climatology of terdiurnal tides using TIMED/SABER observations, Journal of Geophysical Research: Space Physics, 118, 4534–4550, doi:10.1002/jgra.50273.

Namboothiri, S. P., Kishore, P., Murayama, Y., and Igarashi, K., 2004: MF radar observations of Terdiurnal Tide in the mesosphere and lower thermosphere at Wakkanai (45.4°N, 141.7°E), Japan, Journal of Atmospheric and Solar-Terrestrial Physics, 66, 241–250, doi: 10.1016/j.jastp.2003.09.010.

Pancheva, D., Mukhtarov, P., and Smith, A. K., 2013: Climatology of the migrating terdiurnal tide (TW3) in SABER/TIMED temperatures, Journal of Geophysical Research: Space Physics, 118, 1755–1767, doi: 10.1002/jgra.50207.

Pogoreltsev, A. I., Vlasov, A. A., Fröhlich, K., and Jacobi, Ch., 2007: Planetary waves in coupling the lower and upper atmosphere, Journal of Atmospheric and Solar-Terrestrial Physics, 69, 2083 – 2101, doi: 10.1016/j.jastp.2007.05.014.

Randel, W. and Wu, F., 2015: A stratospheric ozone profile data set for 1979–2005: Variability, trends, and comparisons with column ozone data, Journal of Geophysical Research, 112, doi: 10.1029/2006JD007339, Path: ftp://sparc-ftp1.ceda.ac.uk/sparc/ref_clim/ randel/o3data/.

Richards, P. G., Fennelly, J. A., and Torr, D. G., 1994: EUVAC: A Solar EUV Flux Model for aeronomic calculations, Journal of Geophysical Research: Space Physics, 99, 8981–8992, doi:10.1029/94JA00518. (Correction, 1994. J. Geophys. Res. 99, 13283).

Roble, R. G., 1995: Energetics of the Mesosphere and Thermosphere, Geophysical Monographs, 87, 1–21, doi:10.1029/GM087p0001.

Smith, A. K. and Ortland, D. A., 2001: Modeling and Analysis of the Structure and Generation of the Terdiurnal Tide, Journal of the Atmospheric Sciences, 58, 3116–3134, doi: 10.1175/1520-0469(2001)058%3C3116:MAAOTS%3E2.0.CO;2.

Strobel, D. F., 1978: Parameterization of the atmospheric heating rate from 15 to 120 km due to O_2 and O_3 absorption of solar radiation, Journal of Geophysical Research: Oceans, 83, 6225–6230, doi: 10.1029/JC083iC12p06225.

Teitelbaum, H., Vial, F., Manson, A. H., Giraldez, R., and Massebeuf, M., 1989: Non-linear interation between the diurnal and semidiurnal tides: Terdiurnal and diurnal secondary waves, Journal of Atmospheric and Terrestrial Physics, 51, 627–634, doi: 10.1016/0021-9169(89)90061-5.

Yue, J., Xu, J., Chang, L. C., Wu, Q., Liu, H.-L., Lu, X., and Russell III, J., 2013: Global Structure and seasonal variability of the migrating terdiurnal tide in the mesosphere and lower thermosphere, Journal of Atmospheric and Solar-Terrestrial Physics, 105-106, 191–198, doi: 10.1016/j.jastp.2013.10.010.